Original Article

Myocardial extracellular volume fraction analysis in doxorubicin-induced beagle models: comparison of dual-energy CT with equilibrium contrast-enhanced single-energy CT

Zhen Zhou[1], Yifeng Gao[1], Hongwei Wang[1], Wenjing Wang[1], Hongkai Zhang[1], Sicong Wang[2], Zhonghua Sun[3], Lei Xu[1]

[1]Department of Radiology, Beijing Anzhen Hospital, Capital Medical University, Beijing, China; [2]GE Healthcare China, Beijing, China; [3]Discipline of Medical Radiation Sciences, Curtin Medical School, Curtin University, Perth, Australia

Contributions: (I) Conception and design: L Xu, Z Sun; (II) Administrative support: L Xu, Z Sun; (III) Provision of study materials or patients: Z Zhou, Y Gao, H Wang, W Wang, H Zhang; (IV) Collection and assembly of data: Z Zhou, Y Gao, H Wang, W Wang, H Zhang; (V) Data analysis and interpretation: Z Zhou, Y Gao, S Wang; (VI) Manuscript writing: All authors; (VII) Final approval of manuscript: All authors.

Correspondence to: Prof. Lei Xu. Department of Radiology, Beijing Anzhen Hospital, Capital Medical University, No. 2 Anzhen Rd., Chaoyang District, Beijing, 100029, China. Email: leixu2001@hotmail.com; Prof. Zhonghua Sun. Discipline of Medical Radiation Sciences, Curtin Medical School, Curtin University, Perth, Western Australia 6845, Australia. Email: z.sun@curtin.edu.au.

Background: Dual-energy CT (DECT) permits the simultaneous operation of two different kV levels, providing a potential method toward the assessment of diffuse myocardial fibrosis. The purpose of this study was to determine the accuracy of DECT for evaluation of the myocardial extracellular volume (ECV) fraction in comparison with single-energy CT (SECT).

Methods: Myocardial ECV was quantified in fifteen dogs using DECT and dynamic equilibrium SECT before and after doxorubicin administration. Cardiac magnetic resonance imaging (CMRI) was used to assess myocardial function. The histological collagen volume fraction (CVF) was calculated as the gold standard. The Bland-Altman analysis was performed to compare the agreement between DECT-ECV and SECT-ECV. The association among ECV values derived from DECT and SECT, CVF, and left ventricular ejection fraction (LVEF) were determined by correlation analysis. The variations of these values were evaluated using repeated ANOVA.

Results: The DECT- and SECT-ECV were increased with the elongation of modeling time (pre-modeling *vs.* 16-week models *vs.* 24-week models: DECT-ECV 24.1%±1.1%, 35.1%±1.3% and 37.6%±1.4%; SECT-ECV 22.9%±0.8%, 33.6%±1.2% and 36.3%±1.0%; n=30 in per-subject analysis, all $P<0.05$). Both ECV values of DECT and SECT correlated well with the histological CVF results ($R=0.935$ and 0.952 for the DECT-ECV and SECT-ECV; all $P<0.001$; n=13). Bland-Altman plots showed no significant differences between DECT- and SECT-ECV.

Conclusions: DECT-ECV correlated well with both SECT-ECV and histology, showing the feasibility of DECT in evaluating doxorubicin-induced diffuse myocardial interstitial fibrosis.

Keywords: Dual-energy computed tomography (DECT); single-energy computed tomography (SECT); magnetic resonance imaging; extracellular volume fraction (ECV fraction); diffuse myocardial interstitial fibrosis

Submitted Sep 19, 2020. Accepted for publication Dec 28, 2020.
doi: 10.21037/cdt-20-798
View this article at: http://dx.doi.org/10.21037/cdt-20-798

Introduction

Diffuse interstitial myocardial fibrosis is an unfavorable, common endpoint of various cardiomyopathies (CMPs) (1). T1 mapping and myocardial extracellular volume fraction (ECV) derived from cardiac magnetic resonance imaging (CMRI) have been developed to quantify the diffuse myocardial abnormalities with results conformed in both ischemic and nonischemic CMPs (2-5). However, there still have some contraindications and limitations for CMRI (6).

With the advantages of wide availability and high spatial resolution, recently cardiac CT (CCT) has been used for myocardium characterization. Although the ECV derived from non-contrast and delayed-phase CCT has been validated in many conditions, including with high histology and CMR-derived ECV correlations, it is also thought to be of limited use for several reasons. Further, the diagnostic accuracy might be influenced by the differential difficulties between myocardium and blood on pre-contrast CT images, and the misregistration between the pre- and postcontrast CT images (7-9).

With two orthogonally mounted detectors and tube arrays, dual-energy CT (DECT) permits the simultaneous operation of two different kV levels and provides a potential method to measure ECV. DECT acquisition can generate iodine maps and resolve the problem of misregistration. The attenuation values of iodine maps depend on the amount of iodine per voxel (overlay attenuation values in Hounsfield units). Currently, some studies also evaluated the feasibility of DECT-ECV and revealed good agreements with MR imaging findings and histology (10-14).

However, limited studies have been published comparing DECT-ECV directly with ECV values derived from single-energy CT (SECT) on the quantification of diffuse interstitial myocardial fibrosis induced by the cardiotoxic drug. Therefore, the purpose of this study was to test the proof of concept that DECT allows for evaluating the expansion of myocardial ECV fraction induced by doxorubicin with no significant differences between DECT-ECV and SECT measurements. We present the study in accordance with the ARRIVE reporting checklist (available at http://dx.doi.org/10.21037/cdt-20-798).

Methods

Animal experimental settings

Figure 1 shows the detailed animal experiment setup flow. This study was cared for in compliance with the Local Animal Care and Use Committee and the ARRIVE guidelines. In total, 15 female beagles (mean weight 8.5 kg) were selected and all of them were given CMR and CCT scans before doxorubicin administration. Then we randomly selected 3 out of these animals and sacrificed them for pre-modeling histological analysis. The remaining dogs (n=12) received doxorubicin (doxorubicin hydrochloride, Cayman Chemical, Ann Arbor, MI, USA) 30 mg/m^2 intravenously until the cumulative dose reached 240 mg/m^2 (15). Unfortunately, 2 of them suddenly died of acute heart failure during the period of modeling and were excluded from statistical analysis (including their pretreatment images). After 16 weeks, the remaining 10 dogs underwent CMR and CCT scans, and 3 of them were sacrificed for histological biopsy. The rest of the dogs (n=7) continued for myocardial fibrosis modeling and underwent CMR and CCT sans in the 24th week. Finally, all of the remaining dogs (n=7) were sacrificed for histological biopsy.

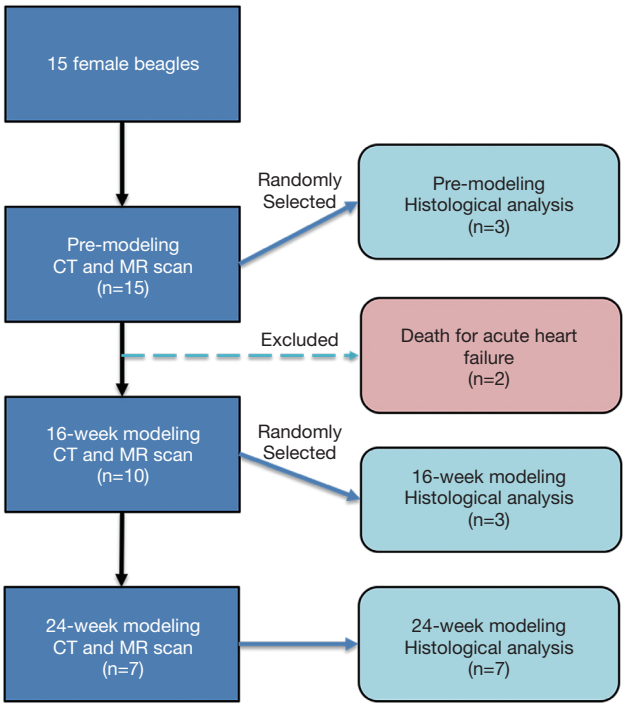

Figure 1 Flow chart of the animals used in the experiment.

Animal preparation for CCT and CMR

In order to induce anesthesia, a mixture of xylazine hydrochloride (2.0 mg/kg, Rompun, Bayer, Seoul, Korea) and ketamine hydrochloride (1.0 mg/kg, Hospira, Lake

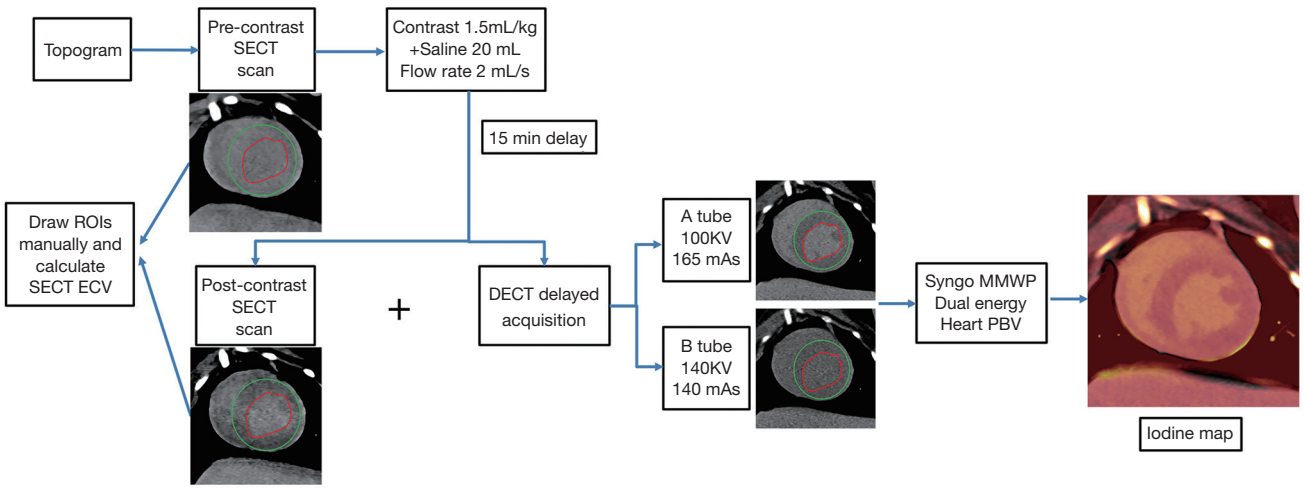

Figure 2 Flowchart of DECT and SECT images acquisition and postprocessing. DECT, dual-energy CT; SECT, single-energy CT.

Forest, CA, USA) was injected intramuscularly. We prepared the forelimb vein of dogs for intravenous contrast agent administration before CCT and CMR examination and collected their blood to measure the hematocrit (Hct) value.

CCT image acquisition

All dogs were examined using a second-generation 128-slice dual-source CT scanner (Somatom Definition Flash; Siemens Healthineers, Forchheim, Germany). The protocols for CCT included an initial survey scan, a pre-contrast and post-contrast SECT scan and a DECT delayed acquisition 15 min after contrast injection. The pre-contrast SECT scan was acquired using a prospective ECG gating, tube voltage of 100 kV with automatically selected tube current, and slice thickness of 0.6 mm. We used iterative reconstruction (SAFIRE, Siemens) to improve image quality with a strength of 3 and a reconstruction increment of 0.4 mm. The post-contrast SECT scan started at 15 min after contrast injection and the scan parameters were identical to those of the pre-contrast SECT acquisition. The DECT scan parameters were as follows: prospective ECG gating with tube current modulation, matrix =512×512, section collimation =64×0.6 mm, tube voltage 140 kV with 140 effective mAs and tube voltage 100 kV with 165 effective mAs, and rotation time =0.28 second. The imaging ranges and the field of views (FOVs) were adjusted according to the dog's heart size. And the slice thickness is 0.6 mm with an increment interval of 0.4 mm for each tube voltage. A medium-smooth convolution kernel B30f was used to reconstruct the axial images at the mid-diastolic phase.

An infusion of 1.5 mL/kg iodinated contrast (370 mg iodine/mL, Ultravist, Bayer Schering Pharma, Berlin, Germany) and 20 mL normal saline was injected intravenously at a flow rate of 2 mL/s using a dual-head power injector (Stellent D, Medrad, Indianola, PA) and automated bolus triggering. Radiation dose estimation was based on the dose length product provided by the scanner and a conversion factor of 0.014 for chest imaging was used (16).

CCT image analysis

A commercial workstation (Syngo MMWP; Siemens Medical Solutions, Forchheim, Germany) was used to post-process all CT data. Two observers, blinded to each dog's findings, drew regions of interest (ROIs) manually on the left ventricle myocardium of reconstructed SECT short-axis images based on AHA 17-segment model (the 17th apex segment excluded for analysis) and the attenuation value of left ventricle cavity (avoiding papillary muscles) was also recorded for calculating the SECT-ECV (*Figure 2*). SECT-ECV was calculated using the following formula:

$$ECV = \left(\frac{\Delta HUmyo}{\Delta HUblood}\right) \times (1 - Hct) \times 100\% \quad [1]$$

where ΔHU_{myo} and ΔHU_{blood} are the differences of myocardium and blood attenuation (Hounsfield units, HU) values between pre-contrast and post-contrast SECT scans.

The low- and high-kVp data of DECT delayed acquisition

were analyzed using a dedicated "Heart PBV (perfused blood volume)" software and the iodine maps, showing the iodine distribution of the entire left ventricle myocardium, were constructed. Similar to SECT images, the reconstruction of iodine maps was also in the short-axis views from base to the apex of the heart with a 6 mm slice thickness and a gap of 0 mm. ROIs were drawn manually in each segment and in the LV blood pool (avoiding the periphery of the myocardium) to obtain the overlay attenuation values (*Figure 2*). The DECT-ECV was calculated as follows:

$$ECV = \left(\frac{HUmyo}{HUblood}\right) \times (1 - Hct) \times 100\% \quad [2]$$

where HU_{myo} and HU_{blood} are the overlay attenuation values of the myocardium ROI (in Hounsfield units) and the blood pool ROI (in Hounsfield units) separately.

CMR image acquisition

CMR examination was obtained using a 3.0T MRI scanner (Verio, Siemens, Erlangen, Germany) with a 32-channel cardiovascular array coil (InVivo, Orlando, FL) after the CCT scan. For the analysis of cardiac function, cine images were acquired using a steady-state free precession (SSFP) sequence and the scan parameters were as follows: TR =45.6 ms, TE =1.66 ms, FOV =219 mm × 260 mm, matrix =256×256 pixels, slice thickness =6 mm, spatial resolution =1.0×0.9 mm^2, flip angle =50°, and average acquisition time =20 seconds per slice. A phase-sensitive inversion recovery prepared SSFP sequence was used to acquire the late gadolinium enhancement (LGE) data and the parameters were as follows: TR =577 ms, TE =1.67 ms, FOV =211 mm × 260 mm, matrix =156×256 pixels, slice thickness was the same as the cine scanning, spatial resolution =1.6×1.0 mm^2, flip angle =20°, and average acquisition time was about 10 seconds per slice. The LGE scan was performed 8 minutes after the 0.15 mmol/kg Gadopentetate dimeglumine administration at a rate of 2.0 mL/s followed by a 10 mL saline flush.

CMR image analysis

To measure the cardiac function, endocardial and epicardial borders of LV myocardium in the short axis view were automatically drawn using dedicated software (Circle Cardiovascular Imaging, CVI42, Caliga, Canada) and papillary muscles were included. The cardiac function parameters included end-diastolic volume (EDV), end-systolic volume (ESV), stroke volume (SV), and left ventricular ejection fraction (LVEF).

Histologic analysis

After CCT and CMR data acquisition, we collected the dogs' samples from the middle LV segments and fixed them in 10% formalin for histology. Sectioning was performed after dehydration and embedding. The corresponding part at the short-axis plane of the mid-LV level was selected using a slice thickness of 5μm followed by the Masson staining. Quantitative analyses were conducted on digital biopsy samples using histology analysis software (Quant center 2.1, 3D HISTECH, Budapest, Hungary). We drawn ROIs manually in a Masson-stained slice of the mid-LV septum myocardium and then calculated the average collagen volume fraction (CVF) of this slice, which was taken as a surrogate of this dog's global CVF value. Two pathologists with 5 years of experience were responsible for analyzing the histological data.

The authors are accountable for all aspects of the work in ensuring that questions related to the accuracy or integrity of any part of the work are appropriately investigated and resolved.

Statistical analysis

Statistical analyses were performed using SPSS (versions 25, Chicago, ILL) and MedCalc (versions 19, Ostend, Belgium). Continuous data with a normal distribution were presented as mean and standard deviations (mean ± SD). Categorical variables were described as frequencies or percentages. We used Bland-Altman plots to analyze the agreement between DECT-ECV and SECT-ECV. The associations among DECT-ECV, SECT-ECV, CVF, and cardiac function indexes were determined by Pearson correlation analysis. The significance of the differences between the two correlation coefficients was tested using the Fisher r-to-z transformation. The variations in CVF values were evaluated using one-way ANOVA, while the changes in DECT-ECV, SECT-ECV, and cardiac function indexes were evaluated using repeated ANOVA. Inter-observer agreement was assessed using the intraclass correlation coefficient (ICC). P values <0.05 was considered statistically significant.

Ethical statement

Experiments were performed under a project license (No.

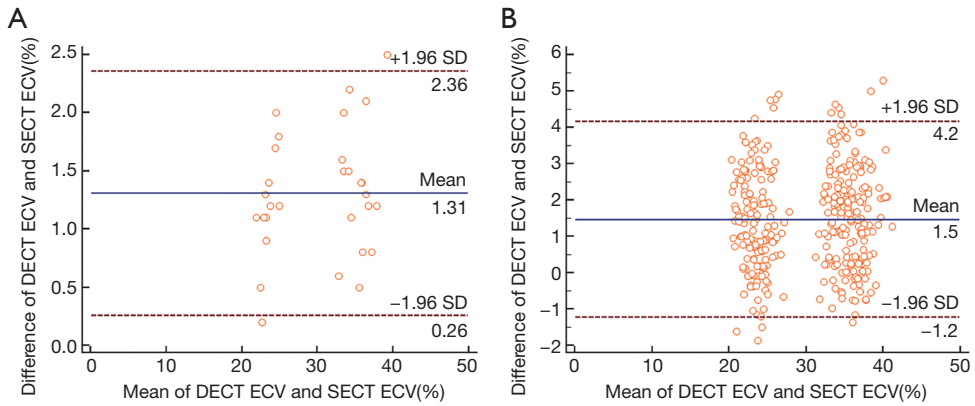

Figure 3 Validation of DECT-ECV vs. SECT-ECV. Bland-Altman plots showed a bias (1.31%) between DECT-ECV and SECT-ECV with 95% limits of agreement from –0.26% to 2.36% in the per-subject analysis (n=30, A) and a bias (1.5%) with 95% limits of agreement from –1.2% to 4.2% in the per-segment analysis (n=360, B). DECT, dual-energy CT; SECT, single-energy CT; ECV, extracellular volume.

2016019X) granted by institutional ethics board of the Animal Care and Use Committee at Anzhen Hospital in Beijing, China, in compliance with the national/institutional guidelines for the care and use of animals.

Results

Comparison of the studied samples

The characteristics of the studied dogs are summarized in *Table 1*. The Hct decreased with the elongation of the modeling time, as well as LVEF, but the EDV and ESV enlarged (n=30 in per subject analysis, all P<0.05). DECT-ECV and SECT-ECV were inversely related to LVEF (n=30, R=–0.744 and –0.746, all P<0.001). The DECT radiation dose of each dog was notably lower than that of SECT (DECT *vs.* SECT 3.1±1.1 *vs.*11.8±3.6 mSv, P<0.001, n=30).

CCT ECV analysis

A total of 480 LV segments of SECT images were analyzed and 390 (81.3%) of those met the diagnostic requirements. Among them, 285 segments (59.4%) were good, 105 (21.9%) were adequate and 90 (16.7%) were poor. Further, 480 LV segments of iodine maps were analyzed for DECT measurements. Of these, 208 (43.3%) were good, 152 (31.7%) were adequate, and 120 (25.0%) were poor. The poor segments were not enrolled in the image analysis.

After doxorubicin injection, both DECT-ECV and SECT-ECV values increased with the duration of the modeling time (DECT-ECV: 24.1%±1.1% for the pre-modeling group, 35.1%±1.3% for the 16th week group and 37.6%±1.4% for the 24th week group; and SECT-ECV: 22.9%±0.8%, 33.6%±1.2%, and 36.3%±1.0%; n=30 in the per-subject analysis, all P<0.05). There is a good correlation between DECT-ECV and SECT-ECV across all the studied dogs (n=30; R=0.986; P<0.001) and all the studied segments (n=360; R=0.976; P<0.001). Between DECT-ECV and SECT-ECV, Bland-Altman plots showed a bias of 1.31% with 95% limits of agreement from –0.26% to 2.36% in the per-subject analysis (n=30) and a bias of 1.5% with 95% limits of agreement from –1.2% to 4.2% in the per-segment analysis (n=360) (*Figure 3*). The correlation coefficients for inter-observer agreement were high (ICC =0.926; 95% CI: 0.867 to 0.955 for DECT-ECV and ICC =0.913; 95% CI: 0.854 to 0.942 for SECT-ECV).

Histology analysis

After doxorubicin administration, the CVF values increased (*Table 1*). Both DECT- ECV and SECT-ECV were positively associated with the histological CVF results (R=0.935 for DECT-ECV; R=0.952 for SECT-ECV; all P<0.001; n=13) and did not differ statistically using Fisher r-to-z transformation (z=–0.35, P=0.73).

Discussion

In this study, we selected 15 beagles with diffuse myocardial fibrosis induced by doxorubicin. ECV fraction was measured on DECT images compared to myocardial fibrosis quantified by equilibrium contrast-enhanced SECT and histology. There are no significant differences between

Table 1 Baseline characteristics of the beagles

Characteristics	Pre-modeling beagles (N=13)	16-week models (N=10)	24-week models (N=7)
Weight (kg)	8.4±1.4	7.1±1.2*	8.8±0.8
Sex	Female	Female	Female
Heart rate (/min)	98±6	86±7	84±8
Hematocrit (%)	49.5±1.6	45.9±1.2*	43.0±1.1#
CVF (%)	3.6±0.8 (N=3)	23.1±1.7 (N=3)*	31.9±2.8 (N=7)#
LV systolic function			
EDV (mL)	24.1±1.7	26.5±0.8*	26.8±1.7#
ESV (mL)	11.6±1.1	14.2±0.6*	15.1±0.8#
SV (mL)	12.5±1.5	12.3±0.7	11.7±1.0
LVEF (%)	51.7±3.9	46.5±2.0*	43.5±1.7#

Values are given as mean ± SD. *, pre-modeling subjects *vs.* 16-week models, P<0.05. #, pre-modeling subjects *vs.* 24-week models, P<0.05. CVF, collagen volume fraction; LV, left ventricle; EDV, end-diastolic volume; ESV, end-systolic volume; SV, stroke volume; LVEF, left ventricular ejection fraction.

DECT-ECV and SECT-ECV. We also revealed a good correlation between DECT-ECV and histologic CVF, highlighting the feasibility of detecting myocardial fibrosis induced by doxorubicin using DECT.

Nowadays, cardiac MR imaging T1 mapping with ECV fraction quantification has been a reliable and reproducible method for assessing diffuse myocardial fibrosis (17,18). Many studies have shown a consistent histologic correlation between T1 mapping and ECV values in a wide range of cardiovascular diseases, including acute and chronic myocardial infarction (19), chronic aortic regurgitation (20), heart failure (21), dilated cardiomyopathy (22), and hypertrophic cardiomyopathy (23). However, CMRI is not widely available, costly, time-consuming, and has certain typical MR-specific contraindications.

Similar to gadolinium-based contrast agent for MRI, the iodinated contrast agent for CT is also an extracellular interstitial agent. Therefore, some researchers have suggested using CCT to characterize myocardial tissue in cases where CMR is not available (7). Compared with CMR, CCT has advantages of quickness, wider availability, and higher spatial resolution (6). At present, two methods of measuring myocardial CT-derived ECV were developed: One is the subtraction-derived method, which can be used with equilibrium contrast-enhanced SECT. This method has been validated in both ischemic cardiomyopathies (CMPs) and non-ischemic CMPs. Treibel *et al*. enrolled 26 patients with cardiac amyloidosis to evaluate the feasibility of equilibrium contrast-enhanced SECT-ECV. They found ECV at SECT correlated well with that at cardiac MR imaging and conventional amyloid measures, suggesting the potential of SECT for myocardial tissue characterization (24). Previous research also investigated the accuracy of ECV measurement of beagle models induced by doxorubicin using equilibrium contrast-enhanced SECT, compared with the reference CMR derived-ECV and histological CVF. Good correlations were also revealed among them, which added further proof of SECT-ECV (25). Additionally, Nacif *et al* also developed a 3D ECV calculation method, which is more efficient and user-friendly than previous 2D measurement (26). However, the subtraction-derived method may be of limited use due to the difficulty in differentiating the myocardium from blood on pre-contrast CT images and the challenge of misregistration between the pre- and postcontrast CT images.

Therefore, another method, iodine density–derived CT ECV emerged. With two orthogonally mounted detectors and tube arrays, DECT has the potential to reduce both beam hardening and metal artifacts and it can generate the iodine maps with overlay attenuation values and provides a potential approach to calculate the ECV values. This method potentially eliminated the requirement for the 2-step process of obtaining pre-contrast and post-contrast images, which avoided misregistration errors and reduced radiation dose. In the study by Lee *et al*., a good agreement between DECT derived-ECV of patients with

non-ischemic cardiomyopathy and MR imaging findings was found, suggesting the potential of diffuse myocardial fibrosis measurement using DECT (14). The study of measuring DECT-ECV fractions in doxorubicin-induced dilated cardiomyopathy rabbit models, designed by Hong *et al*., also revealed that DECT-ECV correlated well with CMR and histology (13). However, the small heart size and fast heart rate or arrhythmia of the rabbits may reduce the quality of DECT images and veracity. Further evidence is needed to verify the ability of DECT in assessing the doxorubicin-induced cardiomyopathy. And limited studies have been published comparing DECT-ECV directly with SECT-ECV on the quantification of diffuse interstitial myocardial fibrosis induced by the cardiotoxic drug.

In this study, we further explored the accuracy of DECT-ECV in evaluating doxorubicin-induced cardiomyopathy. The beagle models were used as they have bigger hearts and thicker myocardium compared with the rabbits. On the condition of medicine administration, the beagle's heart rate is also slower than that of rabbits. The CT images of the dog's heart, with fewer motion artifacts and better quality, improve the reliability of DECT, which may add proof to the use of this technique in assessing the diffuse myocardial fibrosis.

In another study, Assen *et al*. measured the myocardial ECV of patients with suspected coronary artery disease or known cardiomyopathy and found no systematic differences between DECT-ECV and SECT-ECV (10). In this study, we further investigated the difference of doxorubicin-induced myocardial fibrosis quantification using DECT and SECT. And we found no significant difference too. Further, we revealed the increased DECT-ECV values correlated well with reduced cardiac function. This might enable additional DECT evaluation of myocardial fibrosis in various pathological conditions as a part of comprehensive CCT examination and a substitution to CMR in cases where CMR is not available. However, the relatively high radiation exposure should not be ignored.

This study has several limitations. Although eliminating the misregistration errors, the signal-to-noise ratio of DECT images is still inferior to that of CMR, and iodine maps are also prone to artefacts, e.g., beam hardening and streak artefacts that may impede evaluation of myocardial ECV. And the risk of ionizing radiation from DECT cannot be avoided, especially in younger patients when applying our results to patients. Further technical improvements are desirable to lower radiation dose and improve the image quality of the iodine map generated by DECT (6). Further, the small sample size of our study may not be statistically robust or there may be a high risk of model overfitting. Thus, results should be interpreted with caution. Extensive clinical use of DECT-ECV still needs larger clinical studies.

Conclusions

In conclusion, we have performed the assessment of myocardial fibrosis using DECT-ECV. ECV measured with DECT images, with lower radiation dose, shows good reproducibility with no significant difference compared with SECT-ECV. This indicates that DECT represents a potential method for accurate assessment of doxorubicin-induced diffuse myocardial fibrosis.

Acknowledgments

We are grateful to all staff involved in the care of our study subjects.

Funding: This study was supported by research grant from the National Key Research and Development Program of China (2016YFC1300300), research grant from the National Natural Science Foundation of China (U1908211), and research grant from the Capital's Funds for Health Improvement and Research Foundation of China (2020-1-1052) for Dr. Lei Xu.

Footnote

Reporting Checklist: The authors have completed the ARRIVE reporting checklist. Available at http://dx.doi.org/10.21037/cdt-20-798

Data Sharing Statement: Available at http://dx.doi.org/10.21037/cdt-20-798

Conflicts of Interest: All authors have completed the ICMJE uniform disclosure form (Available at http://dx.doi.org/10.21037/cdt-20-798). SW disclosed the personal employment relationship with GE Healthcare Chin. The other authors have no conflicts of interest to declare.

Ethical Statement: The authors are accountable for all aspects of the work in ensuring that questions related to the accuracy or integrity of any part of the work are appropriately investigated and resolved. Experiments were performed under a project license (No. 2016019X) granted by institutional ethics board of the Animal Care and Use

Committee at Anzhen Hospital in Beijing, China, in compliance with the national/institutional guidelines for the care and use of animals.

References

1. Mewton N, Liu CY, Croisille P, et al. Assessment of myocardial fibrosis with cardiovascular magnetic resonance. J Am Coll Cardiol 2011;57:891-903.
2. h-Ici DO, Jeuthe S, Al-Wakeel N, et al. T1 mapping in ischaemic heart disease. Eur Heart J Cardiovasc Imaging 2014;15:597-602.
3. Banypersad SM, Sado DM, Flett AS, et al. Quantification of myocardial extracellular volume fraction in systemic AL amyloidosis: an equilibrium contrast cardiovascular magnetic resonance study. Circ Cardiovasc Imaging 2013;6:34-9.
4. Sado DM, White SK, Piechnik SK, et al. Identification and assessment of Anderson-Fabry disease by cardiovascular magnetic resonance noncontrast myocardial T1 mapping. Circ Cardiovasc Imaging 2013;6:392-8.
5. Swoboda PP, McDiarmid AK, Erhayiem B, et al. Assessing Myocardial Extracellular Volume by T1 Mapping to Distinguish Hypertrophic Cardiomyopathy From Athlete's Heart. J Am Coll Cardiol 2016;67:2189-90.
6. Scully PR, Bastarrika G, Moon JC, et al. Myocardial Extracellular Volume Quantification by Cardiovascular Magnetic Resonance and Computed Tomography. Curr Cardiol Rep 2018;20:15.
7. Nacif MS, Kawel N, Lee JJ, et al. Interstitial myocardial fibrosis assessed as extracellular volume fraction with low-radiation-dose cardiac CT. Radiology 2012;264:876-83.
8. Bandula S, White SK, Flett AS, et al. Measurement of myocardial extracellular volume fraction by using equilibrium contrast-enhanced CT: validation against histologic findings. Radiology 2013;269:396-403.
9. Jablonowski R, Wilson MW, Do L, et al. Multidetector CT measurement of myocardial extracellular volume in acute patchy and contiguous infarction: validation with microscopic measurement. Radiology 2015;274:370-8.
10. van Assen M, De Cecco CN, Sahbaee P, et al. Feasibility of extracellular volume quantification using dual-energy CT. J Cardiovasc Comput Tomogr 2019;13:81-4.
11. Ohta Y, Kishimoto J, Kitao S, et al. Investigation of myocardial extracellular volume fraction in heart failure patients using iodine map with rapid-kV switching dual-energy CT: Segmental comparison with MRI T1 mapping. J Cardiovasc Comput Tomogr 2020;14:349-55.
12. Kumar V, Harfi TT, He X, et al. Estimation of myocardial fibrosis in humans with dual energy CT. J Cardiovasc Comput Tomogr 2019;13:315-8.
13. Hong YJ, Kim TK, Hong D, et al. Myocardial Characterization Using Dual-Energy CT in Doxorubicin-Induced DCM: Comparison With CMR T1-Mapping and Histology in a Rabbit Model. JACC Cardiovasc Imaging 2016;9:836-45.
14. Lee HJ, Im DJ, Youn JC, et al. Myocardial Extracellular Volume Fraction with Dual-Energy Equilibrium Contrast-enhanced Cardiac CT in Nonischemic Cardiomyopathy: A Prospective Comparison with Cardiac MR Imaging. Radiology 2016;280:49-57.
15. Kanter PM, Bullard GA, Ginsberg RA, et al. Comparison of the cardiotoxic effects of liposomal doxorubicin (TLC D-99) versus free doxorubicin in beagle dogs. In Vivo 1993;7:17-26.
16. Hausleiter J, Meyer T, Hermann F, et al. Estimated radiation dose associated with cardiac CT angiography. JAMA 2009;301:500-7.
17. Schelbert EB, Testa SM, Meier CG, et al. Myocardial extravascular extracellular volume fraction measurement by gadolinium cardiovascular magnetic resonance in humans: slow infusion versus bolus. J Cardiovasc Magn Reson 2011;13:16.
18. Ugander M, Oki AJ, Hsu LY, et al. Extracellular volume imaging by magnetic resonance imaging provides insights into overt and sub-clinical myocardial pathology. Eur Heart J 2012;33:1268-78.
19. Messroghli DR, Walters K, Plein S, et al. Myocardial T1 mapping: application to patients with acute and chronic myocardial infarction. Magn Reson Med 2007;58:34-40.
20. Sparrow P, Messroghli DR, Reid S, et al. Myocardial T1 mapping for detection of left ventricular myocardial fibrosis in chronic aortic regurgitation: pilot study. AJR Am J Roentgenol 2006;187:W630-5.
21. Iles L, Pfluger H, Phrommintikul A, et al. Evaluation of diffuse myocardial fibrosis in heart failure with cardiac

magnetic resonance contrast-enhanced T1 mapping. J Am Coll Cardiol 2008;52:1574-80.
22. Han Y, Peters DC, Dokhan B, et al. Shorter difference between myocardium and blood optimal inversion time suggests diffuse fibrosis in dilated cardiomyopathy. J Magn Reson Imaging 2009;30:967-72.
23. Amano Y, Takayama M, Kumita S. Contrast-enhanced myocardial T1-weighted scout (Look-Locker) imaging for the detection of myocardial damages in hypertrophic cardiomyopathy. J Magn Reson Imaging 2009;30:778-84.
24. Treibel TA, Bandula S, Fontana M, et al. Extracellular volume quantification by dynamic equilibrium cardiac computed tomography in cardiac amyloidosis. J Cardiovasc Comput Tomogr 2015;9:585-92.
25. Zhou Z, Xu L, Wang R, et al. Quantification of doxorubicin-induced interstitial myocardial fibrosis in a beagle model using equilibrium contrast-enhanced computed tomography: A comparative study with cardiac magnetic resonance T1-mapping. Int J Cardiol 2019;281:150-5.
26. Nacif MS, Liu Y, Yao J, et al. 3D left ventricular extracellular volume fraction by low-radiation dose cardiac CT: assessment of interstitial myocardial fibrosis. J Cardiovasc Comput Tomogr 2013;7:51-7.

Cite this article as: Zhou Z, Gao Y, Wang H, Wang W, Zhang H, Wang S, Sun Z, Xu L. Myocardial extracellular volume fraction analysis in doxorubicin-induced beagle models: comparison of dual-energy CT with equilibrium contrast-enhanced single-energy CT. Cardiovasc Diagn Ther 2021. doi: 10.21037/cdt-20-798